Global Biogeochemical Cycles

RESEARCH ARTICLE
10.1029/2020GB006760

Key Points:
- Large gradients in dissolved ^{230}Th, ^{231}Pa, and ^{232}Th are found along upwelling isopycnals in the Pacific Southern Ocean
- Zonal variations in Th/Pa fractionation across the Southern Ocean are driven by particle composition
- Isopycnal mixing is of primary importance for transporting ^{231}Pa to the Southern Ocean

Supporting Information:
- Supporting Information S1

Correspondence to:
F. J. Pavia,
fjpavia@caltech.edu

Citation:
Pavia, F. J., Anderson, R. F., Pinedo-Gonzalez, P., Fleisher, M. Q., Brzezinski, M. A., & Robinson, R. S. (2020). Isopycnal transport and scavenging of ^{230}Th and ^{231}Pa in the Pacific Southern Ocean. *Global Biogeochemical Cycles*, *34*, e2020GB006760. https://doi.org/10.1029/2020GB006760

Received 21 JUL 2020
Accepted 2 NOV 2020
Accepted article online 12 NOV 2020

Isopycnal Transport and Scavenging of ^{230}Th and ^{231}Pa in the Pacific Southern Ocean

Frank J. Pavia[1,2,3], Robert F. Anderson[1,2], Paulina Pinedo-Gonzalez[1], Martin Q. Fleisher[1], Mark A. Brzezinski[4], and Rebecca S. Robinson[5]

[1]Lamont-Doherty Earth Observatory, Columbia University, Palisades, NY, USA, [2]Department of Earth and Environmental Sciences, Columbia University, New York, NY, USA, [3]Now at Division of Geological and Planetary Sciences, California Institute of Technology, Pasadena, CA, USA, [4]Marine Science Institute, University of California, Santa Barbara, CA, USA, [5]Graduate School of Oceanography, University of Rhode Island, Narragansett, RI, USA

Abstract The Southern Ocean hosts complex connections between ocean physics, chemistry, and biology. Changes in these connections are hypothesized to be responsible for significant alterations of ocean biogeochemistry and carbon storage both on glacial-interglacial timescales and in the future due to anthropogenic forcing. Isotopes of thorium (^{230}Th and ^{232}Th) and protactinium (^{231}Pa) have been widely applied as tools to study paleoceanographic conditions in the Southern Ocean. However, understanding of the chemical behavior of these isotopes in the modern Southern Ocean has been limited by a paucity of high-resolution observations. In this study, we present measurements of dissolved ^{230}Th, ^{231}Pa, and ^{232}Th on a meridional transect along 170°W from 67°S to 54°S in the Pacific sector of the Southern Ocean, with high vertical and meridional sampling resolution. We find Th/Pa fractionation factors below 1, highlighting the preferential removal of Pa relative to Th in a region with low lithogenic inputs where the particle flux is dominated by biogenic opal. We also find steep gradients in all three of these isotopes along neutral density surfaces from north to south, demonstrating the importance of isopycnal mixing in transporting these nuclides to the Southern Ocean. Our results suggest that ^{231}Pa and ^{230}Th in the Southern Ocean are highly sensitive tracers of physical transport that may find use in studies of Southern Ocean biogeochemical-physical connections in the past, present, and future.

1. Introduction

Southern Ocean circulation is the major global conduit connecting the physical and chemical properties of the deep ocean with the surface ocean and atmosphere. In the Southern Ocean, the divergence caused by easterly winds near the continent and westerly winds offshore upwells nutrient- and carbon-rich deep waters that are carried either southward to form Antarctic Bottom Water around the Antarctic continent (e.g., Marshall & Speer, 2012) or northward where they degas natural CO_2 and take up anthropogenic CO_2 from the atmosphere (Gruber et al., 2009) before subducting to form intermediate and mode waters. Because of limiting levels of iron and light, phytoplankton are unable to fully draw down upwelled dissolved inorganic carbon and nutrients in the surface of the Southern Ocean, causing both intermediate and deep waters to subduct with significant preformed nutrient contents (Sarmiento et al., 2004; Sigman & Boyle, 2000). It is hypothesized that greater nutrient utilization due to enhanced dust inputs and increased stratification in the Southern Ocean led to significant reductions of atmospheric pCO_2 during the last glacial period, stemming the "leak" of CO_2 from the Southern Ocean via reduced ventilation and an increased efficiency of the biological pump (Martínez-Garcia et al., 2014; Siegenthaler & Wenk, 1984; Sigman & Boyle, 2000). Thus, it is critical to study the interactions between physics, chemistry, and biology in the Southern Ocean to understand the global carbon cycle both in the modern ocean and in the geologic past.

The long-lived isotopes of thorium (^{230}Th and ^{232}Th) and protactinium (^{231}Pa) can be used as tracers of particle dynamics and physical transport in both modern and paleo settings with widespread application in the Southern Ocean (e.g., Anderson et al., 2009; Kumar et al., 1993). Primordial ^{232}Th is delivered to the ocean by the dissolution of lithogenic materials, making it a useful tracer for the deposition of continental dust (e.g., Hayes et al., 2013). The radiogenic isotopes ^{230}Th and ^{231}Pa are produced in situ by the decay of uranium (^{234}U → ^{230}Th, ^{235}U → ^{231}Pa). While uranium is highly soluble and well mixed in the oceans, varying only as a function of salinity (Owens et al., 2011), Th and Pa are highly insoluble, with typical water column

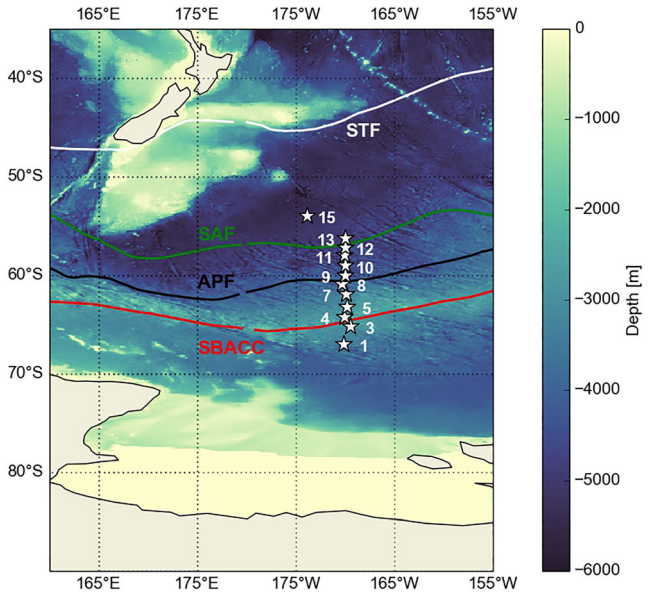

Figure 1. Site map of sampling locations during NBP1702. Individual stations are shown as stars and labeled with their station number. GEBCO 6 × 6 min bathymetry is shown in color. The location of climatological fronts (Orsi et al., 1995) are shown as solid lines, including the Subtropical Front (STF) in white, the Subantarctic Front (SAF) in green, the Antarctic Polar Front (APF) in black, and the Southern Boundary of the Antarctic Circumpolar Current (SBACC) in red.

scavenging residence times of 10–40 years for ^{230}Th and 50–200 years for ^{231}Pa (Henderson & Anderson, 2003) that are much shorter than their respective half-lives of 75,584 years (Cheng et al., 2013) and 32,760 years (Robert et al., 1969). As a result, the vertical scavenging removal of ^{230}Th and ^{231}Pa is nearly quantitative relative to their known water column production rates from U decay. In the absence of lateral redistribution, the burial ratio of ^{231}Pa/^{230}Th would be equal to their water column production ratio (0.093, activity ratio).

Protactinium and thorium have differing sensitivities to many variables that can affect their water column distributions, including particle composition, particle flux, and lateral transport by advection and eddy diffusion. The Southern Ocean is a somewhat unique locale for Pa and Th dynamics. Elevated diatom productivity occurs as nutrient-rich deep waters reach the surface (Nelson et al., 2002), causing diatom opal to dominate the bulk particle flux beneath these areas (Honjo et al., 2000). Biogenic opal has an exceptionally high affinity for removing ^{231}Pa compared to other particle types like lithogenics, $CaCO_3$, and organic matter (e.g., Chase et al., 2002; Geibert & Usbeck, 2004). As a result, ^{231}Pa/^{230}Th ratios in Southern Ocean sediment trap samples (Chase et al., 2003b), in situ pumped particulate matter (Venchiarutti, Roy-Barman, et al., 2011; Walter et al., 1997), and surface sediments (Bradtmiller et al., 2009; Chase et al., 2003b; DeMaster, 1981; Walter et al., 1997) exceed the production ratio of 0.093, necessitating greater net transport of ^{231}Pa into the Southern Ocean compared to ^{230}Th to maintain observed inventories. The close coupling of opal fluxes and ^{231}Pa/^{230}Th ratios has also led to the use of sedimentary ^{231}Pa/^{230}Th as a paleoproxy for past changes in diatom productivity, and thus nutrient supply from upwelling, in the Southern Ocean (Anderson et al., 2009; Kumar et al., 1995).

Previous studies of dissolved and/or total (i.e., dissolved + particulate) ^{231}Pa and ^{230}Th in Southern Ocean waters found negligible meridional gradients along isopycnals for these nuclides, suggesting that southward advection of deep waters, rather than diffusive mixing, is responsible for ^{231}Pa transport into the Southern Ocean (Chase et al., 2003b; Roy-Barman et al., 2019; Rutgers van der Loeff et al., 2016; Rutgers van der Loeff & Berger, 1993; Venchiarutti, Roy-Barman, et al., 2011). However, most of these observations are from the Atlantic sector of the Southern Ocean. Measurements of total ^{231}Pa and ^{230}Th from the Pacific sector had low vertical resolution in the upper 1,500 m (Chase et al., 2003b). Additionally, these studies typically have stations spaced ~5° of latitude apart, preventing identification of gradients on finer scales.

In this study, we measured dissolved ^{231}Pa, ^{230}Th, and ^{232}Th along the NBP1702 section at 170°W in the Southern Ocean. This section reoccupied the Antarctic Environment and Southern Ocean Process (AESOPS) transect from the U.S. Joint Global Ocean Flux Study (JGOSF) program (Smith et al., 2000), where measurements of total ^{231}Pa and ^{230}Th were previously made (Chase et al., 2003b). We first use several measurements of size-fractionated dissolved samples to study the physical speciation of ^{231}Pa and ^{230}Th in near-surface waters. We also present measurements from 12 profiles with an average meridional spacing of ~1° of latitude, with 10–12 measurements in the upper 1,500–2,000 m at each location. At our station furthest to the north, we collected a profile spanning the entire water column (5,247 m). We combine our data with historical sediment trap observations to determine the relative scavenging intensity of ^{231}Pa and ^{230}Th. We document the first evidence for steep north-south isopycnal gradients in dissolved ^{231}Pa and ^{230}Th and find that isopycnal mixing plays an important role in the transport of ^{231}Pa into the Southern Ocean.

2. Materials and Methods

2.1. Cruise Track

The NBP1702 cruise took place aboard the RV *Nathaniel B. Palmer* from McMurdo Station, Antarctica, to Lyttelton, New Zealand, between 24 January and 6 March 2017. Samples were taken along a meridional

transect from 67°S to 54°S at 170°W. This section spanned a variety of physical and biogeochemical regimes, from the Ross Gyre poleward of the Southern Boundary of the Antarctic Circumpolar Current (SBACC); the Antarctic Zone (AZ) between the SBACC and the Antarctic Polar Front (APF); the Polar Frontal Zone (PFZ) between the APF and the Subantarctic Front (SAF); and the Subantarctic Zone north of the SAF (Figure 1).

2.2. Sample Collection and Analysis for dSi and bSi

For biogenic silica concentrations, seawater (1.2 L) was collected from Niskin bottles into polypropylene bottles and filtered through a 1.2-μm pore size polycarbonate filter, placed in a cryovial and dried at 60°C, and analyzed using the alkaline digestion method of Krause et al. (2012). Silicic acid concentrations were measured at sea. Forty milliliters was drawn from the Niskin bottles through silicone tubing into a 50-ml screw-cap polypropylene tube and analyzed as described by Brzezinski and Nelson (1995).

2.3. Sample Collection and Analysis for Th and Pa Isotopes

Most Th and Pa samples were collected in Niskin bottles deployed on a stainless steel rosette. Each sample (~4–5 L) for Th and Pa isotope analysis was filtered through a 0.45-μm Acropak capsule filter into an acid-cleaned cubitainer and acidified to pH = 2 using 6 M hydrochloric acid at sea, following GEOTRACES protocols (Anderson et al., 2012).

In addition, several near-surface seawater samples were collected to determine the size fractionation of dissolved Th and Pa isotopes. These samples were collected using a Perfluoroalkoxy alkane (PFA)-coated Polytetrafluoroethylene (PTFE) bellows pump deployed at approximately 10-m depth, with seawater passed through tubing running from the pump to a clean bubble in the ship's lab. There, approximately 5 L of water was collected for Th and Pa analysis by filtration through either a 0.2- or 0.02-μm capsule filter, collected in an acid-cleaned cubitainer, and acidified to pH = 2 using 6 M hydrochloric acid at sea.

Samples were analyzed onshore using previously published methods for analysis of seawater Th and Pa isotopes at Lamont-Doherty Earth Observatory (Anderson et al., 2012; Pavia et al., 2018, 2019). Samples were spiked with ^{229}Th and ^{233}Pa, added to samples along with 15 mg of dissolved Fe as $Fe(NO_3)_3$, and allowed to equilibrate for 24 h. Sample pH was then raised to pH = 8.3–8.7 by adding ~8–10 ml of concentrated Optima-grade NH_4OH to precipitate Fe as Fe oxyhydroxide. The precipitate was allowed to settle for 2 days. The overlying water was drained, and the Fe precipitate was centrifuged and washed in Milli-Q water before digestion at 200°C in concentrated HNO_3, HF, and $HCLO_4$. After dissolution, the samples were dried down and brought back up in concentrated HCl for separation of Th and Pa fractions via anion exchange chromatography on Bio-Rad AG1-X8 100-200 mesh size resin. Concentrations of ^{230}Th, ^{232}Th, and ^{231}Pa were determined by isotope dilution, with measurements made on a Thermo Element XR Single Collector Magnetic Sector ICP-MS in peak jumping mode.

Procedural blanks were determined by processing 2 L of Milli-Q water in acid-cleaned cubitainers in the same manner as seawater. Blanks were taken to sea and acidified to pH = 2 at the same time as seawater samples and analyzed onshore using identical methods, with two blanks measured for every ~15 samples. Mean and 1σ procedural blanks for dissolved samples were ^{232}Th = 3.7 ± 1.4 pg, ^{230}Th = 0.21 ± 0.06 fg, and ^{231}Pa = 0.03 ± 0.02 fg. Reproducibility was assessed by measuring aliquots of two intercalibrated working standard solutions of ^{232}Th, ^{230}Th, and ^{231}Pa: SW STD 2010-1 (Anderson et al., 2012) and SW STD 2015-1, which has lower ^{232}Th concentrations more similar to Pacific seawater conditions. For standards run alongside NBP1702 samples, the reproducibility for each isotope was 2.12% for ^{230}Th, 0.87% for ^{232}Th, and 1.76% for ^{231}Pa on SW STD 2010-1 and was 0.87% for ^{230}Th, 3.78% for ^{232}Th, and 2.69% for ^{231}Pa on SW STD 2015-1.

Dissolved ^{230}Th and ^{231}Pa were corrected for ingrowth of ^{230}Th and ^{231}Pa during sample storage using the uranium-salinity relationship of Owens et al. (2011), a seawater $^{234}U/^{238}U$ activity ratio of 1.1468 (Andersen et al., 2010), and a seawater $^{238}U/^{235}U$ molar ratio of 137.824 (Weyer et al., 2008). Dissolved ^{230}Th and ^{231}Pa were also corrected for lithogenic contributions using measured dissolved ^{232}Th and assuming a detrital $^{230}Th/^{232}Th$ molar ratio of 4.0×10^{-6} (Roy-Barman et al., 2009) and a $^{231}Pa/^{232}Th$ molar ratio of 8.8×10^{-8}, derived from assuming an average upper continental crust U/Th ratio (Taylor & McLennan, 1995) and secular equilibrium between ^{231}Pa and ^{235}U. Typically, ^{230}Th and ^{231}Pa data corrected in this manner are denoted by the subscript "xs," but since all data shown in this paper have been corrected the same way, we will omit the subscript for clarity.

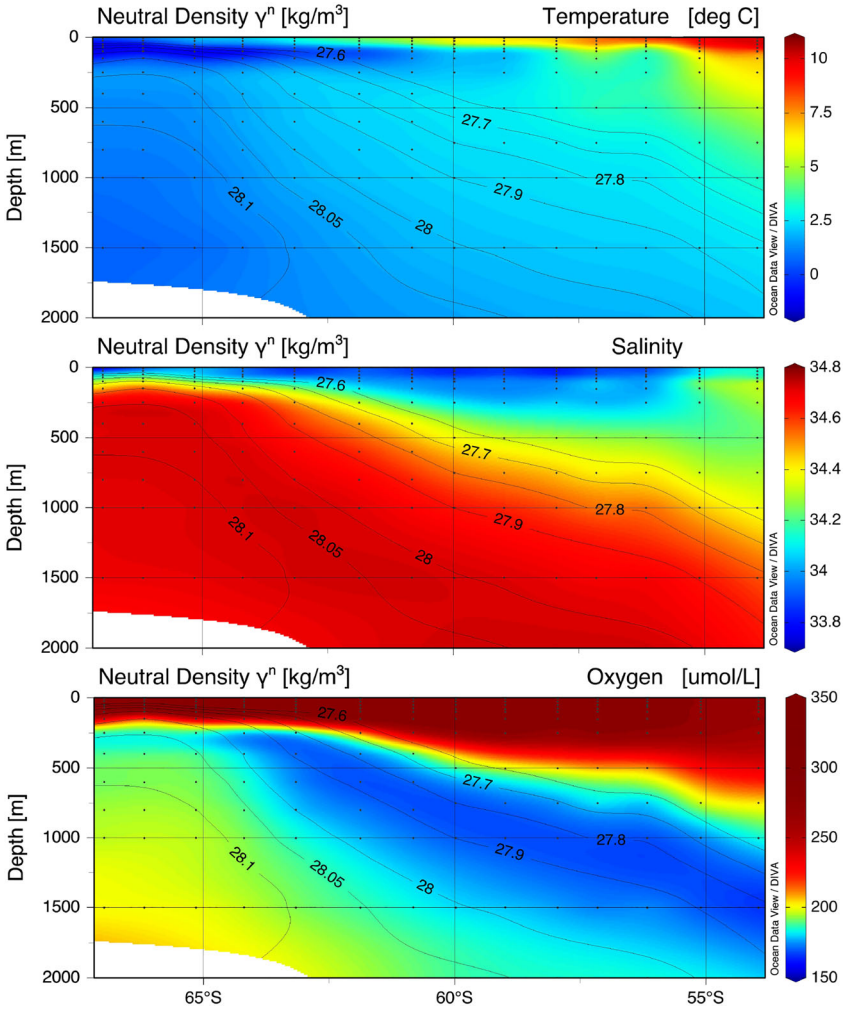

Figure 2. Hydrographic features on the NBP1702 section. (top) CTD temperature, (middle) CTD salinity, and (bottom) CTD oxygen. Individual neutral density surfaces between 27.5 and 28.1 kg m^{-3} are contoured in each panel.

3. Results

3.1. Hydrographic Setting

The Antarctic Circumpolar Current (ACC) is forced by strong westerly surface winds driving divergence and Ekman upwelling, drawing up waters from the deep ocean along isopycnals sloping upward from north to south, resulting in eastward geostrophic flow around the Antarctic continent. The waters upwelling in the Southern Ocean are primarily Circumpolar Deep Water (CDW), which is further subdivided into Upper Circumpolar Deep Water (UCDW; low O_2, high nutrients) and Lower Circumpolar Deep Water (LCDW; higher O_2, higher salinity). On NBP1702, UCDW can be identified by an O_2 minimum between the neutral density surfaces $27.6 \leq \gamma^n \leq 27.95$, sitting above the higher-salinity LCDW found at $\gamma^n > 27.95$ (Figure 2). UCDW and LCDW upwell from below 1,000 m at the northern end of the NBP1702 section to <250-m depth at 65°S where the isopycnals flatten southward (Figure 2).

Above 250 m, waters south of the APF are stratified into two layers typical of austral summer, with warmer, fresher Antarctic Surface Water (AASW) at the surface atop colder, saltier Winter Water (WW) that forms a subsurface temperature minimum at 100×200 m. The WW is a remnant from deep winter mixing (Toole, 1981), while AASW freshens during summer from precipitation and ice melt (Chaigneau et al., 2004; Park et al., 1998). The northward persistence of the subsurface temperature minimum (<2°C) associated with WW can be used to distinguish the northward extent of the APF (Orsi et al., 1995). On NBP1702,

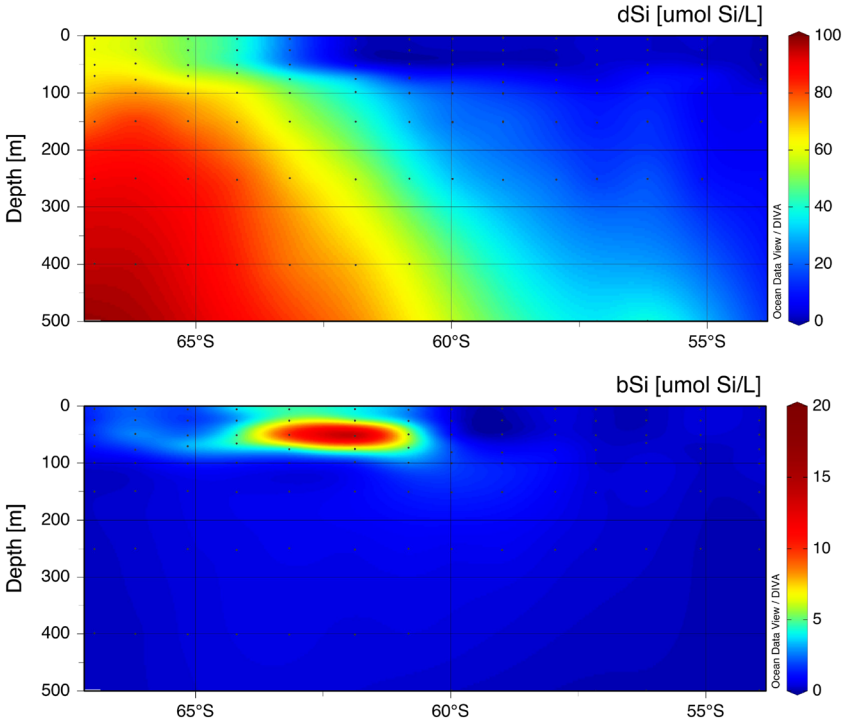

Figure 3. (top) Dissolved $Si(OH)_4$ and (bottom) particulate biogenic silica (bSi) in μmol L^{-1} from the NBP1702 section.

this temperature minimum is found at 59°S (Figure 2), putting the APF ~ 2° further north than in Orsi et al. (1995). This is unlikely to be due to seasonality, as satellite reconstructions of the APF location suggest poleward front migration during austral spring and summer (Freeman et al., 2016).

Ekman upwelling, isopycnal mixing, and deep wintertime diapycnal mixing supply macronutrients and micronutrients like $Si(OH)_4$, NO_3^-, and Fe that fuel diatom productivity. During the winter, more intense mixing, increased ice cover, and low biological uptake allows for net accumulation of nutrients, while intense diatom blooms during spring and summer result in slight NO_3^- drawdown (Morrison et al., 2001) and nearly complete $Si(OH)_4$ drawdown (Sigmon et al., 2002). These blooms result in sharp latitudinal Si $(OH)_4$ gradients in the spring and summer (Brzezinski et al., 2001). On NBP1702, surface $Si(OH)_4$ was below 3 μmol L^{-1} everywhere north of 62°S, sharply increased to 20 μmol L^{-1} at 63°S, and then steadily increased poleward to 61 μmol L^{-1} at 67°S (Figure 3). Continued diatom productivity was evident from ~50-m biogenic silica (bSi) peaks >10 μmol L^{-1} at 62–63°S, with smaller peaks of ~5 μmol L^{-1} at 61°S and 64°S (Figure 3).

3.2. Dissolved ^{230}Th and ^{231}Pa Distributions on NBP1702

Profiles of dissolved ^{230}Th and ^{231}Pa are controlled by the combined influence of circulation and scavenging removal. Profiles of dissolved ^{230}Th and ^{231}Pa typically increase linearly with depth in the upper 2,000 m due to reversible scavenging, reflecting their uniform source in seawater from U decay and equilibrium adsorption/desorption on slow-sinking particles (Bacon & Anderson, 1982). On NBP1702, concave downward profiles of dissolved ^{230}Th, ^{232}Th, and ^{231}Pa occur south of 61°S at Stations 1–7 (Figure 4). These concave profile shapes have previously been found in both the Atlantic and Pacific sectors of the Southern Ocean and reflect upwelling of Th- and Pa-rich deep waters along upward-tilting isopycnals (Chase et al., 2003b; Roy-Barman et al., 2019; Rutgers van der Loeff et al., 2016; Rutgers van der Loeff & Berger, 1993; Venchiarutti, Roy-Barman, et al., 2011). While we were only able to collect samples from the upper 2,000 m for the majority of the cruise, at our station furthest to the north (Station 15, 54°S) we collected a full-depth profile of Th and Pa isotopes. The deep data from Station 15 are not discussed in detail in this paper, but the full-depth profiles of ^{230}Th, ^{231}Pa, and ^{232}Th are included in supporting information Figure S1.

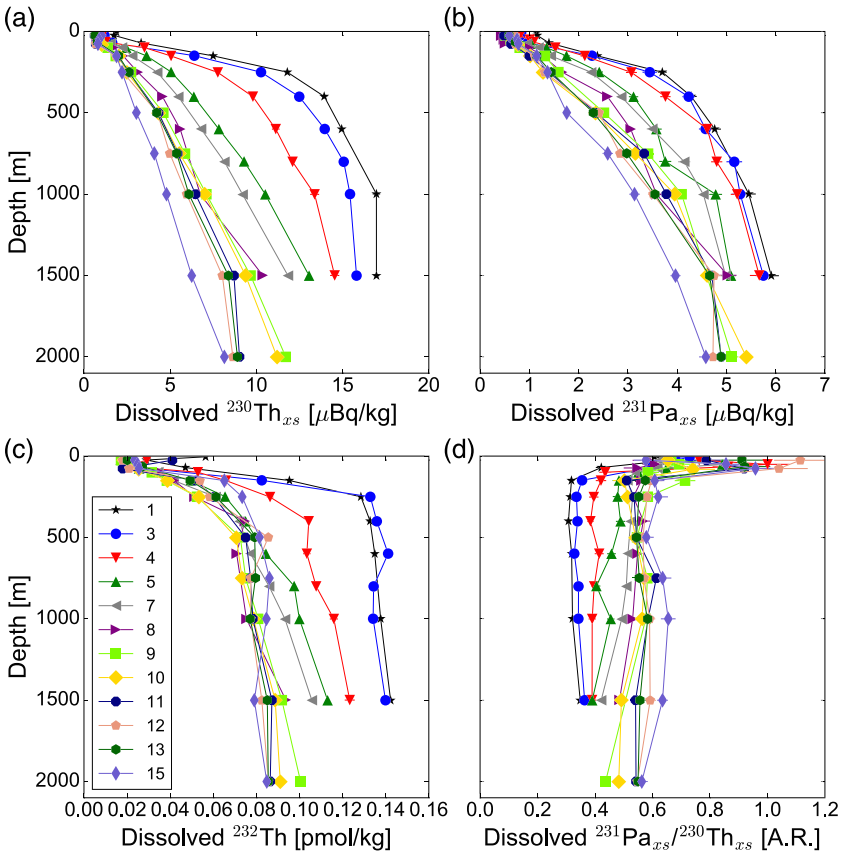

Figure 4. Depth profiles of dissolved (a) ^{230}Th, (b) ^{231}Pa, (c) ^{232}Th, and (d) ^{231}Pa/^{230}Th ratio from NBP1702. The station numbers shown in the legend apply to every panel. Samples were only collected from the upper 1,500–2,000 m for this section, with the exception of Station 15 furthest to the north.

For much of the section north of 61°S, isopleths of ^{230}Th and ^{231}Pa follow neutral density surfaces (Figure 5). The 61–64°S region of most pronounced ^{231}Pa removal directly coincides with the highest levels of biogenic silica measured on the section (Figure 3). Concentrations of ^{230}Th, ^{232}Th, and ^{231}Pa below 100 m increase from north to south, with the largest lateral gradients at depth for ^{230}Th and ^{231}Pa found between ~64°S (Station 4) and ~63°S (Station 5). Dissolved ^{231}Pa/^{230}Th activity ratios decrease from the surface to ~150-m depth, below which the ratios stay constant to 1,000–1,500 m, with values at depth increasing northward from 0.35 at 67°S to 0.6 at 54°S (Figure 4). In the sections below, we explore the impacts of both scavenging and circulation in setting the observed distributions and removal fluxes of Th and Pa isotopes in different sectors of the Southern Ocean.

3.3. Size-Fractionated Dissolved Th and Pa Isotopes

Samples collected via the PFA pump were passed through either a 0.2- or 0.02-μm filter. The ^{230}Th and ^{232}Th concentrations in samples from a given station that were collected using the PFA pump and passed through either a 0.2- or 0.02-μm filter are statistically indistinguishable (Figures 6a and 6c); however, surface samples collected in Niskin bottles and subsequently filtered through 0.45-μm capsule filters were consistently offset higher than samples from the same station collected by the PFA pump and filtered at 0.2 or 0.02 μm, with an offset magnitude averaging 0.4 ± 0.08 μBq kg^{-1} (1σ, n = 6) for ^{230}Th and 0.006 ± 0.003 pmol kg^{-1} (1σ, n = 5) for ^{232}Th. Unlike Th, there is negligible Pa found in any colloidal size class in the NBP1702 samples (Figure 6b). At four of the six stations, %colloidal Pa is statistically indistinguishable from 0 (Figure 6d).

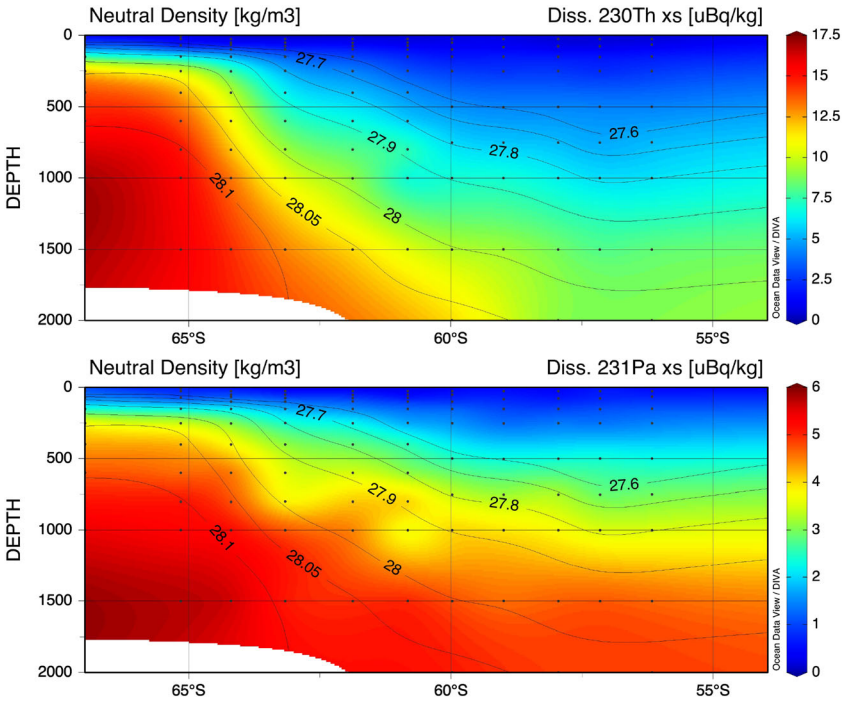

Figure 5. Section plots of dissolved (top) ^{230}Th and (bottom) ^{231}Pa from NBP1702 with neutral density contours.

4. Discussion

4.1. Physical Speciation of Dissolved Th and Pa

We measured the physical speciation of Th and Pa isotopes by measuring size-fractionated dissolved samples passed through different filter sizes. Studying the size speciation of Th and Pa is important for understanding the role of colloids in scavenging (Honeyman et al., 1988; Honeyman & Santschi, 1989) and for testing whether the radiogenic (^{230}Th) and primordial (^{232}Th) are identically scavenged or differentially incorporated into colloids, which would affect estimates of dust deposition based on Th isotopes (Hayes et al., 2013).

Interpreting the partitioning of ^{230}Th and ^{232}Th in size classes <0.45 μm is challenging as the results varied between sampling methods, with the concentrations of both isotopes being higher in samples filtered at 0.45 μm compared to those filtered at either 0.2 or 0.02 μm. Oceanographic interpretation of these results would argue for a significant proportion (up to 60%, Figure 6d) of dissolved Th being present as colloids between 0.2 and 0.45 μm in size, with the rest being soluble (<0.02 μm). This is difficult to reconcile with results from ultrafiltration experiments, where only 10–20% of Th was found to be between 10 kDa and

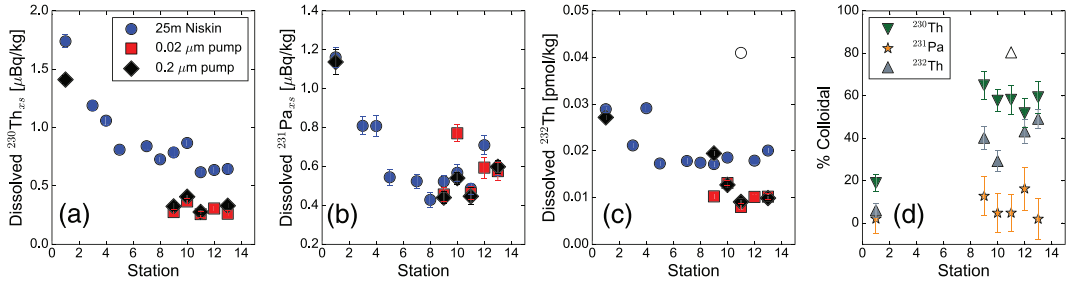

Figure 6. Physical speciation of (a) ^{230}Th, (b) ^{231}Pa, and (c) ^{232}Th in surface samples from the NBP1702 section, as well as (d) apparent percent colloidal. Blue dots show samples collected at 25 m from Niskin bottles and filtered through 0.45-μm Acropak capsule filters. Red squares and black diamonds show samples collected at ~10 m through the PFA pump through 0.02-μm capsule filters and 0.2-μm capsule filters, respectively. Panel (d) shows the percent colloidal in the size range 0.2–0.45 μm calculated for ^{230}Th (blue dots), ^{231}Pa (red diamonds), and ^{232}Th (black squares) on surface samples collected on NBP1702. The ^{232}Th results for the Station 11 sample in panels (c) and (d) are plotted as open symbols, as they were suspected to be ^{232}Th contamination.

0.45 μm in the North Pacific (Hayes, Anderson, Fleisher, Huang, et al., 2015) and <10% of Th was found in the same size class in the subtropical North Atlantic (Hayes et al., 2017).

An alternative explanation for our results is that samples collected by the PFA pump lost Th via adsorption to the sampling apparatus, including the pumping system and the tubing at a constant rate during sampling. During GEOTRACES intercalibration, a small difference in Th concentrations in a 2,000-m sample from the Bermuda Atlantic Time Series filtered at 0.2 and 0.45 μm was observed, though the authors could not conclusively rule out that the difference was due to Th adsorption to the 0.2-μm Osmonics filter cartridge (Anderson et al., 2012). We similarly have difficulty ruling out methodological artifacts as driving the apparently high Th concentrations we observed in the 0.2- to 0.45-μm size class. The concentration of Th in this size class stays mostly constant despite large decreases in surface Th concentrations between Station 1 and Stations 9–13 (Figures 6a–6c). This would imply large increases in the percentage of dissolved Th found as colloids from south to north along the section (Figure 6d).

We attempted to test for adsorption of Th to the plastic PFA pump tubing by analyzing a 0.1 M HCl leachate of tubing used in a subsequent PFA pump deployment. While this acid concentration is fairly dilute, we found vanishingly low concentrations of Th and Pa in the tube leachate, implying that there was insignificant adsorption to plastic tubing during sampling. Future experiments should test whether the apparent colloidal Th signal we observe is real or a methodological artifact by collecting samples using the PFA pump across 0.02-, 0.2-, and 0.45-μm filters or by directly measuring colocated samples collected from Niskin bottles and the PFA pump that are both filtered at 0.45 μm.

We did not detect colloidal Pa, which implies that if a sampling artifact due to adsorption to the apparatus is responsible for the colloidal Th results, that adsorption to tubing does not seem to be an issue for Pa, consistent with previous results finding 15–20 times greater adsorption of Th than Pa to plastic bucket walls during sampling (Anderson et al., 1983a). To the best of our knowledge, these are the first measurements of physical speciation for dissolved ^{231}Pa in the ocean and show that the vast majority of dissolved ^{231}Pa, at least in the Southern Ocean, is not colloidal. This suggests that Pa scavenging in the Southern Ocean is regulated by direct adsorption onto particle surfaces.

4.2. The Role of Particle Composition in Scavenging Th and Pa

Particle composition plays an important role in dictating the removal of Th and Pa from seawater and setting sedimentary ^{231}Pa/^{230}Th ratios. Diatom opal has a particularly high affinity for scavenging ^{231}Pa, and diatom blooms near the APF drive high ^{231}Pa/^{230}Th ratios both in surface sediments (Bradtmiller et al., 2009; Chase et al., 2003b; DeMaster, 1981) and sediment trap particulate material (Chase et al., 2002) in the Southern Ocean. Sedimentary and particulate ^{231}Pa/^{230}Th activity ratios at or above the production ratio of 0.093 in the Southern Ocean are best explained by opal particles having nearly identical affinity for removing Th and Pa from solution (Rutgers van der Loeff & Berger, 1993).

To determine the impact of particle composition in scavenging Th and Pa, we utilize the fractionation factor F(Th/Pa) (Anderson et al., 1983b):

$$F\left(\frac{\mathrm{Th}}{\mathrm{Pa}}\right) = \frac{K_{\mathrm{Th}}}{K_{\mathrm{Pa}}} = \frac{{}^{[\mathrm{Th}]_p}\Big/_{[\mathrm{Th}]_d}}{{}^{[\mathrm{Pa}]_p}\Big/_{[\mathrm{Pa}]_d}} \quad (1)$$

where K refers to the partitioning of the indicated isotope between the particulate (p) and dissolved (d) phases. F(Th/Pa) quantifies the relative scavenging of the two isotopes onto particles. The composition of suspended and sinking particles has been long established as a key variable regulating the relative removal rates of ^{231}Pa and ^{230}Th as particles differ in their relative affinity for the two isotopes depending on their chemical composition. In regions of the ocean where the particle flux is dominated by phases other than opal-like $CaCO_3$, lithogenics, and/or particulate organic carbon, fractionation factors are typically >10, reflecting the greater particle reactivity and shorter scavenging residence time of Th compared to Pa (Hayes, Anderson, Fleisher, Vivancos, et al., 2015; Moran et al., 2002). Areas rich in metalliferous particles have lower fractionation factors, reaching F(Th/Pa) < 5 in the intense Southeast Pacific hydrothermal plume at 15°S (Pavia et al., 2018). The lowest oceanic F(Th/Pa) values have been found in the Southern Ocean, where the particle flux is dominated by opal, indicating that opal is the particle phase with the highest relative affinity for Pa relative to Th.

In the Atlantic sector of the Southern Ocean, F(Th/Pa) is ~2 at the sea surface (Rutgers van der Loeff & Berger, 1993; Venchiarutti, Roy-Barman, et al., 2011) and increases linearly with depth to ~7 at 1,000 m (Venchiarutti, Roy-Barman, et al., 2011). Walter et al. (1997) found lower values of F(Th/Pa) = 1.86 at 700 m near the APF in the Atlantic sector and generally found decreasing F(Th/Pa) from north to south. In the wake of the Kerguelen Plateau, Venchiarutti, Rutgers van der Loeff, et al. (2011) found F(Th/Pa) values as low as 0.06–0.08. Their results were driven by exceptionally high particulate ^{231}Pa concentrations, linked to the intense diatom blooms in this region. In the Pacific Sector on the same 170°W line as the current study, Chase et al. (2002, 2003b) combined annually averaged sediment trap ^{231}Pa/^{230}Th ratios and total (unfiltered) ^{231}Pa/^{230}Th ratios to compute F(Th/Pa) < 1 in the upper 1,000 m at 63°S and 66°S. However, unfiltered samples contain dissolved and particulate Th and Pa and thus are potentially subject to biases when calculating fractionation factors.

We have recalculated F(Th/Pa) values at 170°W using our filtered samples for dissolved ^{230}Th and ^{231}Pa in combination with the sediment trap data from Chase et al. (2002, 2003b). The only location where we sampled at the exact location of the trap moorings is at 63°S. However, several of the other trap moorings were deployed at locations within 110 km of two of our sampling stations. Where this was the case, we interpolated dissolved ^{231}Pa and ^{230}Th between the bracketing stations onto the location of the trap mooring.

We can calculate F(Th/Pa) values in two ways. The first uses the dissolved ^{231}Pa/^{230}Th ratio at the depth of the sediment trap (near 1,000 m), which assumes that the particles in the sediment trap have equilibrated with waters at the same depth. The second uses the dissolved ^{231}Pa/^{230}Th ratio vertically integrated to the depth of the trap, which assumes that the particles in the sediment trap reflect scavenging over the entire water column above the trap depth. The two methods give F(Th/Pa) values that are within 1.5% of each other at all sites—smaller than the relative error of the calculated F(Th/Pa) values. For simplicity we present the F(Th/Pa) results only from the first method in Table 1.

We find F(Th/Pa) values at depths near 1,000 m that decrease from 2.67 at 56.9°S to 0.77 at 63.15°S and 66.16°S (Table 1). The decrease from north to south in F(Th/Pa) coincides with increasing opal contents of the sediment traps. Identical F(Th/Pa) at mooring sites 4 and 5 south of the APF, despite decreasing opal% between the two sites, is likely due to the decrease in $CaCO_3$ (F(Th/Pa) = 33.3; Hayes, Anderson, Fleisher, Vivancos, et al., 2015) and subsequent increase in POM% (F(Th/Pa) = 4.9; Hayes, Anderson, Fleisher, Vivancos, et al., 2015). These F(Th/Pa) values are slightly lower than the original estimate of F(Th/Pa) = 0.88 at 63°S from Chase et al. (2003b) and consistent with preferential removal of Pa relative to Th near and south of the APF at 170°W.

Our results show that there is zonal variability in F(Th/Pa) between the Pacific and Atlantic sectors of the Southern Ocean. This variability is likely not due to greater diatom productivity in the Pacific sector. Annually averaged satellite net primary productivity at the APF (Moore & Abbott, 2002) near 170°W is not substantially higher than that at 0°W (Walter et al., 1997), 50°W (Venchiarutti, Roy-Barman, et al., 2011), or 10–20°E (Rutgers van der Loeff & Berger, 1993). Average sedimentary opal burial rates are statistically indistinguishable between the Pacific and Atlantic sectors of the Southern Ocean (Chase et al., 2015). Instead, we propose that higher F(Th/Pa) in the South Atlantic is due to greater lithogenic dust fluxes compared to that in the South Pacific. The Atlantic sector of the Southern Ocean is downwind of the Patagonian dust plume and is modeled to have ~3–5 times higher dust deposition than at 170°W (Mahowald et al., 2005). Dust flux reconstructions from sub-Antarctic Atlantic coretops are typically 1.5–4 g m^{-2} $year^{-1}$ (Anderson et al., 2014), 3–5 times higher than in the more remote Pacific sector (Chase et al., 2003a). Lithogenic particles have significantly higher affinity for scavenging Th than Pa, with an end-member F(Th/Pa) = 10 (Hayes, Anderson, Fleisher, Vivancos, et al., 2015). Higher dust fluxes in the Atlantic Southern Ocean would cause an increased proportion of the particle flux to be made up of lithogenics than those in the Pacific Southern Ocean, driving higher F(Th/Pa) values.

4.3. Transport of Th and Pa to the Southern Ocean by Isopycnal Mixing

4.3.1. Isopycnal Fluxes of ^{230}Th and ^{231}Pa

Observations of ^{230}Th and ^{231}Pa in the Southern Ocean have been used to construct box models of the transport and burial rates of these nuclides across different fronts and regions of the ACC (Chase et al., 2003b;

Table 1
Particle Composition From Annually Averaged Sediment Trap Deployments Near 1,000 m on NBP9802 (Honjo et al., 2000) and Fractionation Factors F(Th/Pa) Estimated From Pa/Th Values in the Sediment Trap and Dissolved ^{230}Th and ^{231}Pa Measured on NBP1702

Mooring site	Latitude (°N)	Depth (m)	*F*(Th/Pa)	Opal%	$CaCO_3$%	C_{org}%	Lithogenic%
2	−56.90	982	2.67 ± 0.11	52.3	40.6	5.7	0.4
3	−60.28	1,003	1.94 ± 0.09	63.8	29.7	5.4	0.3
4	−63.15	1,031	0.77 ± 0.03	80.6	15.4	3.2	0.2
5	−66.16	937	0.77 ± 0.03	84.7	3.3	10.3	0.3

Note. The particle composition values are calculated as the proportions of each constituent relative to the sum of the measured constituents (also including N_{org} %, not shown here), as described in Honjo et al. (2000).

Rutgers van der Loeff et al., 2016). These models are important for the application of sedimentary ^{231}Pa/^{230}Th ratios as paleoceanographic proxies for opal flux and upwelling in the Southern Ocean (e.g., Anderson et al., 2009; Bradtmiller et al., 2009) and/or deep water flow into the South Atlantic (Negre et al., 2010). The transport modes of ^{230}Th and ^{231}Pa into the Southern Ocean are also important for understanding the processes that close the budgets of these nuclides in both the Pacific (Hayes et al., 2014) and the Atlantic (Deng et al., 2018; Yu et al., 1996). Box models to date typically only consider advection for the meridional transport of Th and Pa toward the Southern Ocean (Luo et al., 2010). This is because dissolved ^{230}Th and ^{231}Pa data from the Southern Ocean have not shown significant gradients along upwelling isopycnals in the upper 1,500 m that would facilitate transport by eddy diffusion, perhaps due either to measurement of total (unfiltered) Th and Pa (Chase et al., 2003b) or to sparse meridional and depth sampling (Chase et al., 2003b; Roy-Barman et al., 2019; Venchiarutti, Roy-Barman, et al., 2011).

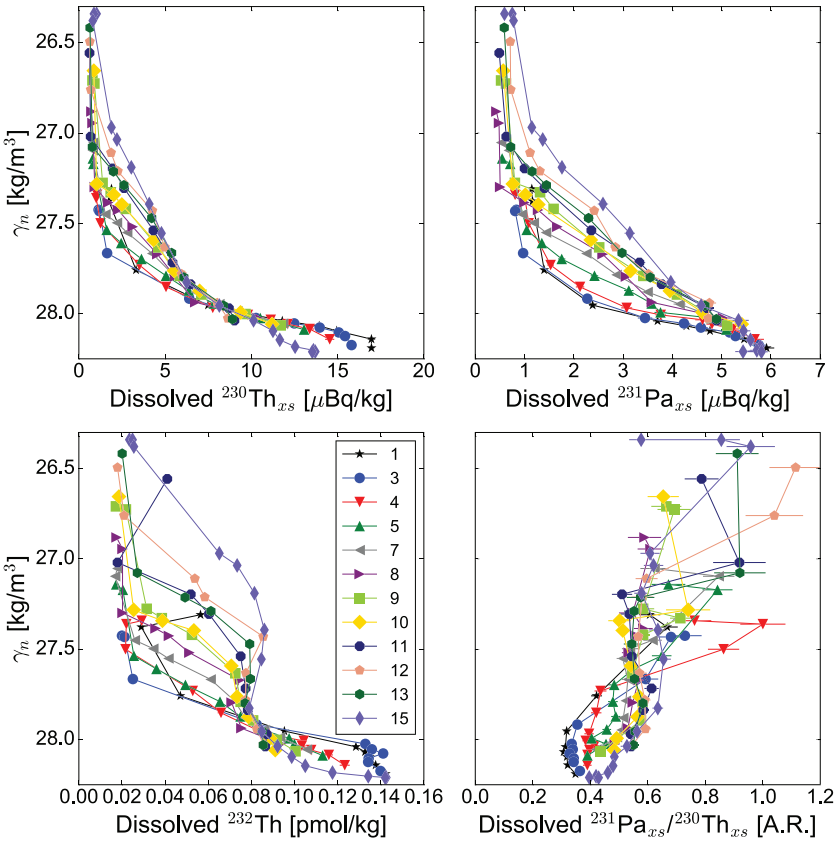

Figure 7. Dissolved Th and Pa isotopes plotted against neutral density, illustrating isopycnal gradients on the NBP1702 section. Panels from left to right show ^{230}Th, ^{231}Pa, ^{232}Th, and the ^{231}Pa/^{230}Th ratio.

On NBP1702, we observe north-south isopycnal gradients for ^{230}Th, ^{231}Pa, and ^{232}Th (Figure 7). North-south gradients along upwelling isopycnals are particularly pronounced for ^{231}Pa, which decreases from north to south at each neutral density level sampled from Station 15 at 54°S to Station 3 at 65°S (Figure 7), with steepest gradients found between density levels $27.5 < \gamma_n < 27.7$ kg m^{-3} and ^{231}Pa values converging between stations toward $\gamma_n \sim 28.1$ kg m^{-3}. Gradients in ^{230}Th and ^{232}Th show similar structure to each other, though the gradients are larger for ^{232}Th than for ^{230}Th, with maximum north-south differences found at $\gamma_n \sim 27.7$ kg m^{-3}. Unlike those in ^{231}Pa, the north–south gradients in ^{230}Th and ^{232}Th converge at $\gamma_n \sim 27.9$ kg m^{-3} and reverse at deeper density levels, with concentrations of both Th isotopes increasing from south to north at $\gamma_n > 27.9$ kg m^{-3} (Figure 7).

The one-dimensional mass balance for dissolved ^{230}Th or ^{231}Pa (A), in steady state, along an isopycnal surface x, can be written as follows:

$$\frac{dA}{dt} = 0 = P - J - u\frac{dA}{dx} + K_h\frac{d^2A}{dx^2} + K_z\frac{d^2A}{dz^2} \quad (2)$$

where P is the production rate from the decay of ^{234}U or ^{235}U, J is the removal rate by particle scavenging, and the third and fourth terms represent dispersive fluxes due to lateral advection along an isopycnal and by eddy diffusion, respectively, where u is the horizontal velocity and K_h is the eddy diffusivity. This equation has been used to calculate lateral fluxes of ^{230}Th from eddy diffusion in boundary scavenging regions in the North Atlantic (Hayes, Fitzsimmons, et al., 2015).

We attempt to determine the role of isopycnal mixing on the budgets of ^{231}Pa and ^{230}Th in the SW Pacific Southern Ocean using a similar approach. We estimate the role of eddy diffusion following the approach of Hayes, Fitzsimmons, et al. (2015); however, we also outline a few ways this approach may be too simplistic and could be improved upon. Our assumption of one-dimensional dynamics may not be appropriate in the ACC, which is dominated by strong zonal transport. Features observed on a given meridional section may be inherited in part from upstream biogeochemical processes. Calculating the second derivative $\frac{d^2A}{dx^2}$ is done on discrete density levels and requires determining the length scales over which eddy diffusion acts on the tracers, with diffusion parameterized as a random-walk process: $\Delta x = \sqrt{2K_h\tau}$, where τ is the water column residence time of ^{230}Th or ^{231}Pa. Hayes, Fitzsimmons, et al. (2015) determined τ by dividing water column inventories of dissolved ^{230}Th and ^{231}Pa by their integrated water column production rates. However, in boundary scavenging regions where there is net lateral influx (outflux) of a nuclide, this approach to determining residence times will overestimate (underestimate) the true residence time. Additionally, the integrated residence times of ^{231}Pa and ^{230}Th increase with depth, which should increase the length scale on which eddy diffusion acts to transport ^{230}Th and ^{231}Pa; however, in their approach, a single length scale was used for determining lateral gradients. A final caveat that becomes important in the Southern Ocean is that eddy diffusivities vary as a function of both depth and latitude (e.g., Abernathey et al., 2010; Chapman & Sallée, 2017). This makes the selection of a single eddy diffusivity to compute lateral fluxes extremely complex and possibly makes the formulation of the diffusive fluxes incorrect, depending on the significance of the meridional gradients in eddy diffusivity.

A few of these issues can be circumvented in the Southern Ocean, though not all. For instance, the depth-integrated residence time of ^{230}Th and ^{231}Pa on NBP1702 cannot be determined a priori given the influence of lateral transport apparent in their concave profiles (Figure 4) and uncertainties in the local eddy diffusivities. However, since F(Th/Pa) is close to 1 averaged over the upper 1,000 m at 63°S (see section 4.2), we assert that the scavenging residence times and thus the diffusive length scales of ^{230}Th and ^{231}Pa are similar in this region. We use an estimate of $K_h = 1{,}000$ m^2 s^{-1} at 170°W on the $\gamma_n = 27.9$ kg m^{-3} isopycnal (Chapman & Sallée, 2017) as representative for each of the isopycnals chosen, while acknowledging that this is a simplification with ~50% uncertainty. For now, we also assume constant residence times on each isopycnal of ~15 years for both isotopes, giving a resulting diffusive length scale $\Delta x \sim 1{,}000$ km. On NBP1702, 1,000 km is the latitudinal distance between Stations 3 and 13, and we choose Station 8 as the intermediate station between the two. Were there more station combinations spaced at the appropriate diffusive length scale, the following calculations would be possible there as well.

Table 2
Second Isopycnal Gradients of ^{230}Th and ^{231}Pa on Six Different Neutral Density Surfaces, As Well As the ^{231}Pa/^{230}Th Diffusive Transport Ratio, Evaluated at NBP1702 Station 8

Neutral density level (kg m^{-3})	^{230}Th lateral diffusive flux convergence (μBq m^{-3} year^{-1})	^{230}Th production rate (μBq m^{-3} year^{-1})	^{231}Pa lateral diffusive flux convergence (μBq m^{-3} year^{-1})	^{231}Pa production rate (μBq m^{-3} year^{-1})	^{231}Pa/^{230}Th transport ratio (activity ratio)
27.5	37.6	433.1	−4.0	40.28	−0.11
27.6	179.1	433.1	90.2	40.28	0.50
27.7	237.3	433.1	152.6	40.28	0.64
27.8	153.9	433.1	141.1	40.28	0.92
27.9	152.0	433.1	205.1	40.28	1.35
28.0	79.2	433.1	172.9	40.28	2.18

We multiply the calculated second isopycnal gradients by the lateral eddy diffusivity of 1,000 m^2 s^{-1} to derive the flux convergence of ^{230}Th and ^{231}Pa due to isopycnal mixing at 63°S (Table 2). The volume-specific mixing fluxes (μBq m^{-3} year^{-1}) of ^{230}Th peak on the 27.7 kg m^{-3} neutral density surface, with maximum values that are ~55% of the local production rate by ^{234}U decay, suggesting that isopycnal mixing is a significant source of ^{230}Th to the Pacific Southern Ocean. To quantify the net effect of isopycnal mixing on the depth-integrated ^{230}Th budget, we integrate the discrete volume-specific isopycnal flux divergences at Station 8 with depth. This depth-integrated ^{230}Th flux from isopycnal mixing at 1,360 m is 172.2 mBq m^{-2} year^{-1}, which is 30% of the integrated production rate from ^{234}U decay. Particle fluxes derived from ^{230}Th-normalization performed at 1,360 m would thus be biased by 30% due to isopycnal diffusive ^{230}Th transport alone. Future work characterizing the full-depth water column will be needed to determine the net effect of isopycnal mixing on ^{230}Th burial rates in the Pacific Southern Ocean. If the supply of ^{230}Th to the Southern Ocean were to vary through time, either due to changes in scavenging-driven meridional ^{230}Th gradients or via wind-driven changes in isopycnal mixing rates (Abernathey & Ferreira, 2015), so too would its burial rate, potentially complicating its use as a constant flux proxy for sediment mass accumulation rates in this region (Costa et al., 2020).

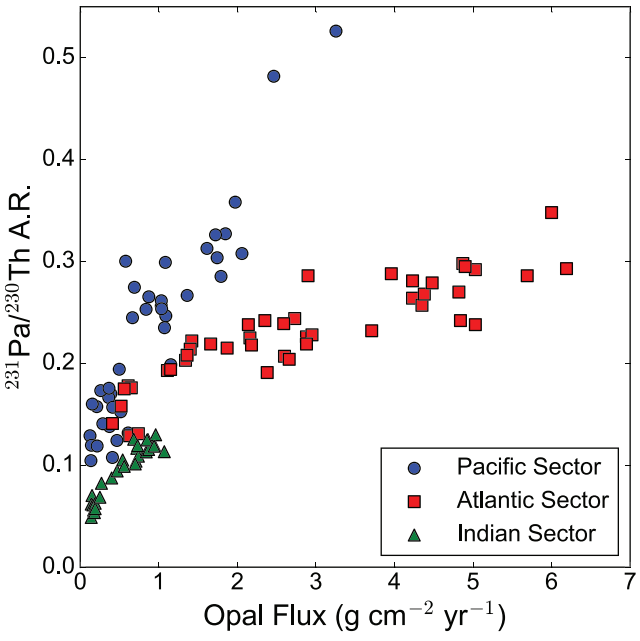

Figure 8. Downcore sedimentary ^{231}Pa/^{230}Th activity ratios and biogenic opal fluxes from south of the Antarctic Polar Front in the Atlantic (TN057-13-4PC; Anderson et al., 2009), Indian (E27-23, Anderson et al., 2009), and Pacific (NBP9802-5PC, NBP9802-6PC, and NBP9802-7PC; Chase et al., 2003a) sectors of the Southern Ocean.

Isopycnal transport plays an even greater role in the budget of ^{231}Pa. The volume-specific mixing fluxes (μBq m^{-3} year^{-1}) on a given isopycnal peak at γ_n = 27.9 kg m^{-3}, with maximum fluxes 5 times higher than its production rate from ^{235}U decay (Table 2). The depth-integrated ^{231}Pa isopycnal mixing flux at 1,360 m is 179.5 mBq m^{-2} year^{-1}, 3.3 times higher than its water column production rate. At each density surface below γ_n = 27.6 kg m^{-3}, the ^{231}Pa/^{230}Th transport ratio greatly exceeds the water column production ratio of 0.093. Together, these results suggest that lateral mixing along upwelling isopycnals is of primary importance in supplying ^{231}Pa to the Pacific sector of the Southern Ocean from lower latitudes.

4.3.2. Mechanisms for Interbasin Differences in Mixing Transport

The importance of mixing in transporting ^{231}Pa along isopycnals into the Pacific Southern Ocean can be seen in sedimentary ^{231}Pa/^{230}Th ratios. To illustrate this, we compare the downcore relationship between ^{231}Pa/^{230}Th ratios and opal burial rates between sediment cores from different sectors of the Southern Ocean, all south of the APF (Figure 8): TN057-13-4PC from the Atlantic sector (Anderson et al., 2009); E27-23 from the Indian sector (Anderson et al., 2009); and NBP9802-5PC, NBP9802-6PC, and NBP9802-7PC from the Pacific sector (Chase et al., 2003a). The slope of the ^{231}Pa/^{230}Th vs. opal flux relationship is greatest for the Pacific sector (Figure 8), implying that for a given change in opal flux, more ^{231}Pa is removed from the Pacific sector of the Southern Ocean to be scavenged and buried relative to ^{230}Th. This effect is not due to differential opal preservation, as opal preservation efficiencies are similar among the sectors

of the Southern Ocean (Sayles et al., 2001). Instead, this difference reflects the unique capacity of isopycnal mixing to enhance the supply ^{231}Pa into the Pacific sector over the Atlantic sector of the Southern Ocean.

The large dissolved ^{231}Pa gradients in the Southern Ocean are due to scavenging by biogenic opal, which has an order of magnitude higher distribution coefficient (K_d) for Pa scavenging than any other major particle phase (Chase et al., 2003b). The very high affinity of opal for Pa scavenging and abundance of diatom productivity in the Southern Ocean is what establishes the larger meridional concentration gradient for Pa than for Th in the Southern Ocean. Mean opal burial rates are similar in both the Atlantic and Pacific sectors (Chase et al., 2015), so meridional dissolved ^{231}Pa gradients should be similar as well.

We argue that the interbasin difference in Pa transport is due to differences in particle composition in the Atlantic and Pacific Southern Oceans, most notably the much higher dust flux in the Atlantic discussed in section 4.2. We hypothesize that the higher dust flux in the Atlantic sector increases the scavenging rate of Th, driving larger meridional isopycnal gradients and greater southward supply of ^{230}Th by lateral mixing compared to those in the Pacific sector. This difference in ^{230}Th supply between the Atlantic and the Pacific is thus the driver of the lower ^{231}Pa/^{230}Th ratios observed for a given opal flux in the Atlantic compared to those in the Pacific (Figure 8). In the modern water column, the higher dust fluxes in the Atlantic sector of the Southern Ocean are what drive the higher F(Th/Pa) there than in the Pacific sector, as discussed in section 4.2. We do not wish to imply that ^{230}Th is not efficiently scavenged in the Pacific Southern Ocean, as Chase et al. (2003b) found that 70–90% of the ^{230}Th production above 1,000 m was scavenged locally in bottom-moored sediment traps. Rather, we suggest that ^{231}Pa is scavenged exceptionally efficiently throughout the Southern Ocean and that ^{230}Th is scavenged more efficiently in the Atlantic sector than in the Pacific sector because of higher dust fluxes. The source of this extra ^{230}Th transported to the Atlantic sector is yet unclear—whether it is from the north, the south, or export out of the Pacific basin. Additional work will be needed to determine the meridional and zonal transport of ^{230}Th into the Atlantic Southern Ocean.

Future modeling work to construct complete ^{231}Pa and ^{230}Th budgets may provide unique constraints on the rates of isopycnal upwelling and mixing in the Southern Ocean. Additionally, our results suggest that reconstruction of the changing ratios between sedimentary ^{231}Pa/^{230}Th and opal flux may provide an avenue to reconstruct the efficiency of isopycnal mixing in supplying tracers from the ocean interior to the surface of the Southern Ocean, a physical processes that is critical for ventilating the modern deep ocean (Jones & Abernathey, 2019) but has yet to be reconstructed for past climates.

5. Summary and Outlook

Our high-resolution measurements from 170°W offer new insights into the dynamics of scavenging and physical transport of ^{231}Pa and ^{230}Th in the Southern Ocean. There is intriguing evidence for unique physical speciation of ^{230}Th in large colloids, but methodological artifacts cannot definitively be ruled out as a cause of the finding. More work will be required to determine whether adsorption onto one or more components of the sampling apparatus caused samples collected by the PFA pump to have lower Th concentrations and whether this is an issue for other reactive trace metals. We found fractionation factors F (Th/Pa) less than 1 in the upper 1,000 m south of the APF, indicating that ^{231}Pa is more efficiently scavenged than ^{230}Th. In combination with the lack of colloidal Pa, this is strong evidence for direct adsorption of Pa to opal surfaces as being the dominant driver of scavenging in the Pacific Southern Ocean. Lower F (Th/Pa) values in the Pacific sector than in the Atlantic sector are consistent with higher coretop ^{231}Pa/^{230}Th ratios in the Pacific. This difference may be due to greater dust deposition in the Atlantic sector, with the higher dust/opal ratio of particulate material in the Atlantic sector driving higher fractionation factors. The data also suggest that the magnitude of the fractionation factor in the Southern Ocean is key in setting the gradients in ^{231}Pa and ^{230}Th along neutral density surfaces from north to south, thereby modulating the role of isopycnal mixing in transporting these nuclides to the Southern Ocean. In the Pacific, fractionation factors <1 drive strong isopyncal gradients in ^{231}Pa, causing the isopyncal flux to greatly exceed the production by U decay. Future work incorporating ^{230}Th and ^{231}Pa into global models would allow for quantification of the net transport of ^{230}Th and ^{231}Pa to the Southern Ocean due to both advective upwelling and isopycnal mixing.

The importance of mixing in transporting ^{231}Pa toward the Southern Ocean should be taken into account both in mass balances of ^{231}Pa in ocean basins (Deng et al., 2018; Hayes et al., 2014) and in paleoceanographic studies of ^{231}Pa burial in the Southern Ocean (Anderson et al., 2009). More complex models of these nuclides could be developed by combining our measurements with transports from the Southern Ocean State Estimate (Mazloff et al., 2010) to constrain isopycnal diffusivities and removal rates. Our results present exciting new opportunities for applying measurements of ^{231}Pa and ^{230}Th to study Southern Ocean physics and biogeochemistry in modern and paleo-oceans.

Data Availability Statement

Dissolved Th and Pa data are available online through BCO-DMO (at https://www.bco-dmo.org/dataset/813379). Dissolved and biogenic silica data can be found online (at https://www.usap-dc.org/view/dataset/601269), and CTD data can be found through MGDS (at http://www.marine-geo.org/tools/entry/NBP1702).

Acknowledgments
This work was supported by U.S. National Science Foundation grant OPP-1542962 to LDEO and an NSF Graduate Research Fellowship to F. J. P. (DGE-1644869). We thank the captain and crew of the R/V *Nathaniel B. Palmer* for their support in difficult conditions on the NBP1702 cruise. Discussions with Spencer Jones and Sophie Hines improved the quality of the paper, as did comments from Matthieu Roy-Barman and an anonymous reviewer.

References

Abernathey, R., & Ferreira, D. (2015). Southern Ocean isopycnal mixing and ventilation changes driven by winds. *Geophysical Research Letters*, *42*, 10,357–10,365. https://doi.org/10.1002/2015GL066238

Abernathey, R., Marshall, J., Mazloff, M., & Shuckburgh, E. (2010). Enhancement of mesoscale eddy stirring at steering levels in the Southern Ocean. *Journal of Physical Oceanography*, *40*(1), 170–184. https://doi.org/10.1175/2009JPO4201.1

Andersen, M. B., Stirling, C. H., Zimmermann, B., & Halliday, A. N. (2010). Precise determination of the open ocean ^{234}U/^{238}U composition. *Geochemistry Geophysics Geosystems*, *11*, Q12003. https://doi.org/10.1029/2010GC003318

Anderson, R. F., Ali, S., Bradtmiller, L. I., Nielsen, S. H. H., Fleisher, M. Q., Anderson, B. E., & Burckle, L. H. (2009). Wind-driven upwelling in the Southern Ocean and the deglacial rise in atmospheric CO_2. *Science*, *323*(5920), 1443–1448. https://doi.org/10.1126/science.1167441

Anderson, R. F., Bacon, M. P., & Brewer, P. G. (1983a). Removal of ^{230}Th and ^{231}Pa from the open ocean. *Earth and Planetary Science Letters*, *62*(1), 7–23. https://doi.org/10.1016/0012-821X(83)90067-5

Anderson, R. F., Bacon, M. P., & Brewer, P. G. (1983b). Removal of ^{230}Th and ^{231}Pa at ocean margins. *Earth and Planetary Science Letters*, *66*, 73–90. https://doi.org/10.1016/0012-821X(83)90127-9

Anderson, R. F., Barker, S., Fleisher, M., Gersonde, R., Goldstein, S. L., Kuhn, G., et al. (2014). Biological response to millennial variability of dust and nutrient supply in the Subantarctic South Atlantic Ocean. *Philosophical Transactions of the Royal Society A: Mathematical, Physical and Engineering Sciences*, *372*(2019), 20130054. https://doi.org/10.1098/rsta.2013.0054

Anderson, R. F., Fleisher, M. Q., Robinson, L. F., Edwards, R. L., Hoff, J. A., Moran, S. B., et al. (2012). GEOTRACES intercalibration of ^{230}Th, ^{232}Th, ^{231}Pa, and prospects for ^{10}Be. *Progress in Oceanography*, *10*(4), 179–213. https://doi.org/10.4319/lom.2012.10.179

Bacon, M. P., & Anderson, R. F. (1982). Distribution of thorium isotopes between dissolved and particulate forms in the Deep Sea. *Journal of Geophysical Research*, *87*(C3), 2045–2056. https://doi.org/10.1111/j.1365-3091.2012.01327.x

Bradtmiller, L. I., Anderson, R. F., Fleisher, M. Q., & Burckle, L. H. (2009). Comparing glacial and Holocene opal fluxes in the Pacific sector of the Southern Ocean. *Paleoceanography*, *24*, PA2214. https://doi.org/10.1029/2008PA001693

Brzezinski, M. A., & Nelson, D. M. (1995). The annual silica cycle in the Sargasso Sea near Bermuda. *Deep Sea Research Part I: Oceanographic Research Papers*, *42*(7), 1215–1237. https://doi.org/10.1016/0967-0637(95)93592-3

Brzezinski, M. A., Nelson, D. M., Franck, V. M., & Sigmon, D. E. (2001). Silicon dynamics within an intense open-ocean diatom bloom in the Pacific sector of the Southern Ocean. *Deep Sea Research Part II: Topical Studies in Oceanography*, *48*(19–20), 3997–4018. https://doi.org/10.1016/S0967-0645(01)00078-9

Chaigneau, A., Morrow, R. A., & Rintoul, S. R. (2004). Seasonal and interannual evolution of the mixed layer in the Antarctic Zone south of Tasmania. *Deep Sea Research Part I: Oceanographic Research Papers*, *51*(12), 2047–2072. https://doi.org/10.1016/j.dsr.2004.06.013

Chapman, C., & Sallée, J.-B. (2017). Isopycnal mixing suppression by the Antarctic Circumpolar Current and the Southern Ocean meridional overturning circulation. *Journal of Physical Oceanography*, *47*(8), 2023–2045. https://doi.org/10.1175/JPO-D-16-0263.1

Chase, Z., Anderson, R. F., Fleisher, M. Q., & Kubik, P. W. (2002). The influence of particle composition and particle flux on scavenging of Th, Pa and Be in the ocean. *Earth and Planetary Science Letters*, *204*(1–2), 215–229. https://doi.org/10.1016/S0012-821X(02)00984-6

Chase, Z., Anderson, R. F., Fleisher, M. Q., & Kubik, P. W. (2003a). Accumulation of biogenic and lithogenic material in the Pacific sector of the Southern Ocean during the past 40,000 years. *Deep Sea Research Part II: Topical Studies in Oceanography*, *50*(3), 799–832.

Chase, Z., Anderson, R. F., Fleisher, M. Q., & Kubik, P. W. (2003b). Scavenging of ^{230}Th, ^{231}Pa and ^{10}Be in the Southern Ocean (SW Pacific sector): The importance of particle flux, particle composition and advection. *Deep Sea Research Part II: Topical Studies in Oceanography*, *50*(3–4), 739–768. https://doi.org/10.1016/S0967-0645(02)00593-3

Chase, Z., Kohfeld, K. E., & Matsumoto, K. (2015). Controls on biogenic silica burial in the Southern Ocean. *Global Biogeochemical Cycles*, *29*, 1599–1616. https://doi.org/10.1002/2015GB005186

Cheng, H., Lawrence Edwards, R., Shen, C. C., Polyak, V. J., Asmerom, Y., Woodhead, J., et al. (2013). Improvements in ^{230}Th dating, ^{230}Th and ^{234}U half-life values, and U–Th isotopic measurements by multi-collector inductively coupled plasma mass spectrometry. *Earth and Planetary Science Letters*, *371–372*, 82–91. https://doi.org/10.1016/j.epsl.2013.04.006

Costa, K. M., Hayes, C. T., Anderson, R. F., Pavia, F. J., Bausch, A., Deng, F., et al. (2020). ^{230}Th normalization: New insights on an essential tool for quantifying sedimentary fluxes in the modern and Quaternary ocean. *Paleoceanography and Paleoclimatology*, *35*, 387. https://doi.org/10.1029/2019PA003820

DeMaster, D. J. (1981). The supply and accumulation of silica in the marine environment. *Geochimica et Cosmochimica Acta*, *45*(10), 1715–1732. https://doi.org/10.1016/0016-7037(81)90006-5

Deng, F., Henderson, G. M., Castrillejo, M., Perez, F. F., & Steinfeldt, R. (2018). Evolution of ^{231}Pa and ^{230}Th in overflow waters of the North Atlantic. *Biogeosciences*, *15*(23), 7299–7313. https://doi.org/10.5194/bg-15-7299-2018

Freeman, N. M., Lovenduski, N. S., & Gent, P. R. (2016). Temporal variability in the Antarctic Polar Front (2002–2014). *Journal of Geophysical Research: Oceans*, *121*, 7263–7276. https://doi.org/10.1002/2016JC012145

Geibert, W., & Usbeck, R. (2004). Adsorption of thorium and protactinium onto different particle types: Experimental findings. *Geochimica et Cosmochimica Acta*, *68*(7), 1489–1501. https://doi.org/10.1016/j.gca.2003.10.011

Gruber, N., Gloor, M., Mikaloff Fletcher, S. E., Doney, S. C., Dutkiewicz, S., Follows, M. J., et al. (2009). Oceanic sources, sinks, and transport of atmospheric CO_2. *Global Biogeochemical Cycles*, *23*, GB1005. https://doi.org/10.1029/2008GB003349

Hayes, C. T., Anderson, R. F., Fleisher, M. Q., Huang, K.-F., Robinson, L. F., Lu, Y., et al. (2015). ^{230}Th and ^{231}Pa on GEOTRACES GA03, the U.S. GEOTRACES North Atlantic transect, and implications for modern and paleoceanographic chemical fluxes. *Deep Sea Research Part II: Topical Studies in Oceanography*, *116*, 29–41. https://doi.org/10.1016/j.dsr2.2014.07.007

Hayes, C. T., Anderson, R. F., Fleisher, M. Q., Serno, S., Winckler, G., & Gersonde, R. (2013). Quantifying lithogenic inputs to the North Pacific Ocean using the long-lived thorium isotopes. *Earth and Planetary Science Letters*, *383*, 16–25. https://doi.org/10.1016/j.epsl.2013.09.025

Hayes, C. T., Anderson, R. F., Fleisher, M. Q., Serno, S., Winckler, G., & Gersonde, R. (2014). Biogeography in ^{231}Pa/^{230}Th ratios and a balanced ^{231}Pa budget for the Pacific Ocean. *Earth and Planetary Science Letters*, *391*, 307–318. https://doi.org/10.1016/j.epsl.2014.02.001

Hayes, C. T., Anderson, R. F., Fleisher, M. Q., Vivancos, S. M., Lam, P. J., Ohnemus, D. C., et al. (2015). Intensity of Th and Pa scavenging partitioned by particle chemistry in the North Atlantic Ocean. *Marine Chemistry*, *170*, 49–60. https://doi.org/10.1016/j.marchem.2015.01.006

Hayes, C. T., Fitzsimmons, J. N., Boyle, E. A., McGee, D., Anderson, R. F., Weisend, R., & Morton, P. L. (2015). Thorium isotopes tracing the iron cycle at the Hawaii Ocean Time-series Station ALOHA. *Geochimica et Cosmochimica Acta*, *169*, 1–16. https://doi.org/10.1016/j.gca.2015.07.019

Hayes, C. T., Rosen, J., McGee, D., & Boyle, E. A. (2017). Thorium distributions in high- and low-dust regions and the significance for iron supply. *Global Biogeochemical Cycles*, *31*, 328–347. https://doi.org/10.1002/2016GB005511

Henderson, G. M., & Anderson, R. F. (2003). The U-series toolbox for paleoceanography. *Reviews in Mineralogy and Geochemistry*, *52*(1), 493–531. https://doi.org/10.2113/0520493

Honeyman, B. D., Balistrieri, L. S., & Murray, J. W. (1988). Oceanic trace-metal scavenging—The importance of particle concentration. *Deep Sea Research Part A. Oceanographic Research Papers*, *35*(2), 227–246.

Honeyman, B. D., & Santschi, P. H. (1989). A Brownian-pumping model for oceanic trace metal scavenging: Evidence from Th isotopes. *Journal of Marine Research*, *47*(4), 951–992. https://doi.org/10.1357/002224089785076091

Honjo, S., Francois, R., Manganini, S., Dymond, J., & Collier, R. (2000). Particle fluxes to the interior of the Southern Ocean in the western Pacific sector along 170°W. *Deep Sea Research Part II: Topical Studies in Oceanography*, *47*(15–16), 3521–3548. https://doi.org/10.1016/S0967-0645(00)00077-1

Jones, C. S., & Abernathey, R. P. (2019). Isopycnal mixing controls deep ocean ventilation. *Geophysical Research Letters*, *42*, 13,144–13,151. https://doi.org/10.1029/2019GL085208

Krause, J. W., Brzezinski, M. A., Villareal, T. A., & Wilson, C. (2012). Increased kinetic efficiency for silicic acid uptake as a driver of summer diatom blooms in the North Pacific subtropical gyre. *Limnology and Oceanography*, *57*(4), 1084–1098. https://doi.org/10.4319/lo.2012.57.4.1084

Kumar, N., Anderson, R. F., Mortlock, R. A., Froelich, P. N., Kubik, P., Dittrich-Hannen, B., & Suter, M. (1995). Increased biological productivity and export production in the glacial Southern Ocean. *Nature*, *378*(6558), 675–680. https://doi.org/10.1038/378675a0

Kumar, N., Gwiazda, R., Anderson, R. F., & Froelich, P. N. (1993). ^{231}Pa/^{230}Th ratios in sediments as a proxy for past changes in Southern Ocean productivity. *Nature*, *362*(6415), 45–48. https://doi.org/10.1038/362045a0

Luo, Y., François, R., & Allen, S. E. (2010). Sediment ^{231}Pa/^{230}Th as a recorder of the rate of the Atlantic meridional overturning circulation: Insights from a 2-D model. *Ocean Science*, *6*(1), 381–400. https://doi.org/10.5194/os-6-381-2010

Mahowald, N. M., Baker, A. R., Bergametti, G., Brooks, N., Duce, R. A., Jickells, T. D., et al. (2005). Atmospheric global dust cycle and iron inputs to the ocean. *Global Biogeochemical Cycles*, *19*, GB4025. https://doi.org/10.1029/2004GB002402

Marshall, J., & Speer, K. (2012). Closure of the meridional overturning circulation through Southern Ocean upwelling. *Nature Geoscience*, *5*(3), 171–180. https://doi.org/10.1038/ngeo1391

Martínez-Garcia, A., Sigman, D. M., Ren, H., Anderson, R. F., Straub, M., Hodell, D. A., et al. (2014). Iron fertilization of the Subantarctic ocean during the last ice age. *Science*, *343*(6177), 1347–1350. https://doi.org/10.1126/science.1246848

Mazloff, M. R., Heimbach, P., & Wunsch, C. (2010). An eddy-permitting Southern Ocean state estimate. *Journal of Physical Oceanography*, *40*(5), 880–899. https://doi.org/10.1175/2009JPO4236.1

Moore, J. K., & Abbott, M. R. (2002). Surface chlorophyll concentrations in relation to the Antarctic Polar Front: Seasonal and spatial patterns from satellite observations. *Journal of Marine Systems*, *37*(1–3), 69–86. https://doi.org/10.1016/S0924-7963(02)00196-3

Moran, S. B., Shen, C. C., Edmonds, H. N., Weinstein, S. E., Smith, J. N., & Edwards, R. L. (2002). Dissolved and particulate ^{231}Pa and ^{230}Th in the Atlantic Ocean: Constraints on intermediate/deep water age, boundary scavenging, and ^{231}Pa/^{230}Th fractionation. *Earth and Planetary Science Letters*, *203*(3–4), 999–1014. https://doi.org/10.1016/S0012-821X(02)00928-7

Morrison, J. M., Gaurin, S., Codispoti, L. A., Takahashi, T., Millero, F. J., Gardner, W. D., & Richardson, M. J. (2001). Seasonal evolution of hydrographic properties in the Antarctic circumpolar current at 170°W during 1997–1998. *Deep Sea Research Part II: Topical Studies in Oceanography*, *48*(19–20), 3943–3972. https://doi.org/10.1016/S0967-0645(01)00075-3

Negre, C., Zahn, R., Thomas, A. L., Masqué, P., Henderson, G. M., Martínez-Méndez, G., et al. (2010). Reversed flow of Atlantic deep water during the Last Glacial Maximum. *Nature*, *468*(7320), 84–88. https://doi.org/10.1038/nature09508

Nelson, D. M., Anderson, R. F., Barber, R. T., Brzezinski, M. A., Buesseler, K. O., Chase, Z., et al. (2002). Vertical budgets for organic carbon and biogenic silica in the Pacific sector of the Southern Ocean, 1996–1998. *Deep Sea Research Part II: Topical Studies in Oceanography*, *49*(9–10), 1645–1674. https://doi.org/10.1016/S0967-0645(02)00005-X

Orsi, A. H., Whitworth, T. III, & Nowlin, W. D. Jr. (1995). On the meridional extent and fronts of the Antarctic Circumpolar Current. *Deep Sea Research Part I: Oceanographic Research Papers*, *42*(5), 641–673. https://doi.org/10.1016/0967-0637(95)00021-W

Owens, S. A., Buesseler, K. O., & Sims, K. W. W. (2011). Re-evaluating the ^{238}U-salinity relationship in seawater: Implications for the ^{238}U–^{234}Th disequilibrium method. *Marine Chemistry*, *127*(1–4), 31–39. https://doi.org/10.1016/j.marchem.2011.07.005

Park, Y. H., Charriaud, E., & Fieux, M. (1998). Thermohaline structure of the Antarctic Surface Water/Winter Water in the Indian sector of the Southern Ocean. *Journal of Marine Systems*, *17*(1–4), 5–23. https://doi.org/10.1016/S0924-7963(98)00026-8

Pavia, F., Anderson, R., Vivancos, S., Fleisher, M., Lam, P., Lu, Y., et al. (2018). Intense hydrothermal scavenging of ^{230}Th and ^{231}Pa in the deep Southeast Pacific. *Marine Chemistry*, *201*, 212–228. https://doi.org/10.1016/j.marchem.2017.08.003

Pavia, F. J., Anderson, R. F., Black, E. E., Kipp, L. E., Vivancos, S. M., Fleisher, M. Q., et al. (2019). Timescales of hydrothermal scavenging in the South Pacific Ocean from ^{234}Th, ^{230}Th, and ^{228}Th. *Earth and Planetary Science Letters*, *506*, 146–156. https://doi.org/10.1016/j.epsl.2018.10.038

Robert, J., Miranda, C. F., & Muxart, R. (1969). Mesure de la période du protactinium 231 par microcalorimétrie. *Radiochimica Acta*, *11*(2), 104–108. https://doi.org/10.1524/ract.1969.11.2.104

Roy-Barman, M., Lemaître, C., Ayrault, S., Jeandel, C., Souhaut, M., & Miquel, J. C. (2009). The influence of particle composition on thorium scavenging in the Mediterranean Sea. *Earth and Planetary Science Letters*, *286*(3–4), 526–534. https://doi.org/10.1016/j.epsl.2009.07.018

Roy-Barman, M., Thil, F., Bordier, L., Dapoigny, A., Foliot, L., Ayrault, S., et al. (2019). Thorium isotopes in the Southeast Atlantic Ocean: Tracking scavenging during water mass mixing along neutral density surfaces. *Deep Sea Research Part I: Oceanographic Research Papers*, *149*, 103042. https://doi.org/10.1016/j.dsr.2019.05.002

Rutgers van der Loeff, M., Venchiarutti, C., Stimac, I., van Ooijen, J., Huhn, O., Rohardt, G., & Strass, V. (2016). Meridional circulation across the Antarctic Circumpolar Current serves as a double ^{231}Pa and ^{230}Th trap. *Earth and Planetary Science Letters*, *455*, 73–84. https://doi.org/10.1016/j.epsl.2016.07.027

Rutgers van der Loeff, M. M., & Berger, G. W. (1993). Scavenging of ^{230}Th and ^{231}Pa near the Antarctic Polar Front in the South Atlantic. *Deep Sea Research Part I: Oceanographic Research Papers*, *40*(2), 339–357. https://doi.org/10.1016/0967-0637(93)90007-P

Sarmiento, J. L., Gruber, N., Brzezinski, M. A., & Dunne, J. P. (2004). High-latitude controls of thermocline nutrients and low latitude biological productivity. *Nature*, *427*(6969), 56–60. https://doi.org/10.1038/nature02127

Sayles, F. L., Martin, W. R., Chase, Z., & Anderson, R. F. (2001). Benthic remineralization and burial of biogenic SiO_2, $CaCO_3$, organic carbon, and detrital material in the Southern Ocean along a transect at 170° west. *Deep Sea Research Part II: Topical Studies in Oceanography*, *48*(19–20), 4323–4383. https://doi.org/10.1016/S0967-0645(01)00091-1

Siegenthaler, U., & Wenk, T. (1984). Rapid atmospheric CO_2 variations and ocean circulation. *Nature*, *308*(5960), 624–626. https://doi.org/10.1038/308624a0

Sigman, D. M., & Boyle, E. A. (2000). Glacial/interglacial variations in atmospheric carbon dioxide. *Nature*, *407*(6806), 859–869. https://doi.org/10.1038/35038000

Sigmon, D. E., Nelson, D. M., & Brzezinski, M. A. (2002). The Si cycle in the Pacific sector of the Southern Ocean: Seasonal diatom production in the surface layer and export to the deep sea. *Deep Sea Research Part II: Topical Studies in Oceanography*, *49*(9–10), 1747–1763. https://doi.org/10.1016/S0967-0645(02)00010-3

Smith, W. O. Jr., Anderson, R. F., Keith Moore, J., Codispoti, L. A., & Morrison, J. M. (2000). The US Southern Ocean Joint Global Ocean Flux study: An introduction to AESOPS. *Deep Sea Research Part II: Topical Studies in Oceanography*, *47*(15–16), 3073–3093. https://doi.org/10.1016/S0967-0645(00)00059-X

Taylor, S. R., & McLennan, S. M. (1995). The geochemical evolution of the continental crust. *Reviews of Geophysics*, *33*(2), 241. https://doi.org/10.1029/95RG00262

Toole, J. M. (1981). Sea ice, winter convection, and the temperature minimum layer in the Southern Ocean. *Journal of Geophysical Research*, *86*(C9), 8037–8047. https://doi.org/10.1029/JC086iC09p08037

Venchiarutti, C., Roy-Barman, M., Freydier, R., van Beek, P., Souhaut, M., & Jeandel, C. (2011). Influence of intense scavenging on Pa-Th fractionation in the wake of Kerguelen Island (Southern Ocean). *Biogeosciences*, *8*(11), 3187–3201. https://doi.org/10.5194/bg-8-3187-2011

Venchiarutti, C., Rutgers van der Loeff, M., & Stimac, I. (2011). Scavenging of ^{231}Pa and thorium isotopes based on dissolved and size-fractionated particulate distributions at Drake Passage (ANTXXIV-3). *Deep Sea Research Part II: Topical Studies in Oceanography*, *58*(25–26), 2767–2784. https://doi.org/10.1016/j.dsr2.2010.10.040

Walter, H. J., Rutgers van der Loeff, M. M., & Hoeltzen, H. (1997). Enhanced scavenging of ^{231}Pa relative to ^{230}Th in the South Atlantic south of the Polar Front: Implications for the use of the ^{231}Pa/^{230}Th ratio as a paleoproductivity proxy. *Earth and Planetary Science Letters*, *149*(1–4), 85–100. https://doi.org/10.1016/S0012-821X(97)00068-X

Weyer, S., Anbar, A. D., Gerdes, A., Gordon, G. W., Algeo, T. J., & Boyle, E. A. (2008). Natural fractionation of ^{238}U/^{235}U. *Geochimica et Cosmochimica Acta*, *72*(2), 345–359. https://doi.org/10.1016/j.gca.2007.11.012

Yu, E.-F., Francois, R., & Bacon, M. P. (1996). Similar rates of modern and last-glacial ocean thermohaline circulation inferred from radiochemical data. *Nature*, *379*(6567), 689–694. https://doi.org/10.1038/379689a0